Origins of structural and electrochemical influence on Y-doped BaZrO[3] heat-treated with NiO additive

AUTHOR(S):

Han, Donglin; Shinoda, Kozo; Tsukimoto, Susumu; Takeuchi, Hisao; Hiraiwa, Chihiro; Majima, Masatoshi; Uda, Tetsuya

CITATION:

Han, Donglin ...[et al]. Origins of structural and electrochemical influence on Y-doped BaZrO[3] heat-treated with NiO additive. Journal of Materials Chemistry A 2014, 2(31): 12552-12560

ISSUE DATE:

2014-05-29

URL:

http://hdl.handle.net/2433/198561

To: Journal of Materials Chemistry A

Origins of Structural and Electrochemical Influence on Y-doped $BaZrO_3$ Heat-treated with NiO Additive

Donglin Han [a*], Kozo Shinoda [b], Susumu Tsukimoto [c], Hisao Takeuchi [d], Chihiro Hiraiwa [d], Masatoshi Majima [d], Tetsuya Uda [a*]

[a] Department of Materials Science and Engineering, Kyoto University,

Yoshida Honmachi, Sakyo-ku, Kyoto 606-8501, Japan

[b] Institute of Multidisciplinary Research for Advanced Materials, Tohoku University,

Katahira 2-1-1, Aoba-ku, Sendai 980-8577, Japan

[c] Advanced Institute for Materials Research, Tohoku University,

Katahira 2-1-1, Aoba-ku, Sendai 980-8577, Japan

[d] Sumitomo Electric Industries, Ltd.,

1-1-1, Koyakita, Itami-shi, Hyogo 664-0016, Japan

* Corresponding author: Donglin Han (han.donglin.8n@kyoto-u.ac.jp)

and Tetsuya Uda (materials_process@aqua.mtl.kyoto-u.ac.jp)

TEL: +81-75-753-5445, FAX: +81-75-753-5284

Abstract

Nickel (Ni) is expected to be an attractive anode material for protonic ceramic fuel cells using Y-doped $BaZrO_3$ (BZY) as an electrolyte, since Ni shows good catalytic property for anode reaction, and NiO is a sintering aid for BZY. In this work, a systematic investigation was performed to reveal the influence of Ni incorporation on structural and electrochemical properties of BZY. Then, some new knowledge was obtained; the important point is that Ni cations occupy the interstitial position of $(\frac{1}{2}, 0, 0)$ in the lattice of BZY, with a greatly Ba-deficient environment. As the results, Ba cations were possibly driven to the grain boundary and induced the formation of a liquid phase, which promoted the sintering process. However, the occupation of Ni on this $(\frac{1}{2}, 0, 0)$ position also resulted in a negative influence on conductivity. A careful processing is required to apply Ni as the electrode in BZY based fuel cells.

Keywords: $BaZrO_3$, Nickel, Fuel cell, EXAFS, XANES, Proton conductor

1. Introduction

Protonic ceramic fuel cells (PCFCs) using proton conductive oxides as electrolytes are promising devices for energy conversion, due to their relatively low operation temperature (400 – 700 ^{o}C), and high fuel utilization. [1] Among various electrolyte candidates, Y-doped $BaZrO_3$ (BZY20) exhibits advantages of both high protonic conductivity and excellent chemical stability [2-4], and therefore receives growing attention [5-11]. Considerable efforts have been focused on the fabrication of anode-supported PCFCs [7-11], in which a mixture of BZY and Ni metal particles is generally applied as a composite anode to maintain the mechanical strength of the fuel cells, and thereby enables depositing a very thin electrolyte layer with low ohmic resistance.

In a conventional preparation method for these anode-supported fuel cells, co-sintering the BZY – NiO anode substrate with the BZY electrolyte is usually examined. But in such process, Ni cations in the anode substrate diffuse into the BZY electrolyte, which obviously lowers the performance of the PCFCs [7, 12]. Ni metal is no doubt a very promising anode material due to its low cost and good catalytic property for anode reaction. Thus, the chemical compatibility between Ni and BZY is a very interesting topic.

In addition, BZY is known for its refractory nature. Sintering temperature higher than 1600 ^{o}C is needed for its densification and grain growth. [13, 14] But NiO acts as an effective sintering additive for BZY, and the sintering temperature can be lowered down to around 1400 ^{o}C [13, 15].

A tentative mechanism for the sintering behaviour with NiO additive was suggested by Tong *et al*. [16, 17]

Understanding the reaction mechanism between BZY and NiO is highly important not only for improving the sinterability, but also for elevating the fuel cell performance. The present work therefore aims to clarify the influence of dissolved NiO on conductivity and water content, and the crystallographic position and oxidation state of Ni in BZY, in order to understand the reaction between NiO and BZY.

2. Experimental

2.1 Material preparation

Samples were prepared by a conventional solid state reaction method. Nominal cation ratios of Ba : Zr : Y of 1.0 : 0.8 : 0.2 and 1.2 : 0.8 : 0.2 were achieved by mixing the starting materials of $BaCO_3$, ZrO_2, and Y_2O_3 at the desired ratios. We named them as $BaZr_{0.8}Y_{0.2}O_{3-\delta}$ (BZY20) and $Ba_{1.2}Zr_{0.8}Y_{0.2}O_{3-\delta}$ for convenience. Mixtures were ball-milled for 24 h, and pressed into pellets under 9.8 MPa and heat-treated at 1000 ^{o}C for 10 h. After ball-milling for 10 h, samples were pressed into pellets under 9.8 MPa again, and kept at 1300 ^{o}C for 10 h for synthesizing. The samples were subsequently ball-milled for 50 h.

The BZY20 powder synthesized at 1300 ^{o}C was then mixed with NiO powder at a molar ratio of 100 mol ($BaZr_{0.8}Y_{0.2}O_{3-\delta}$) to n mol (NiO, n = 0.5, 1, 2, 5, 10). In the following text, these samples were

named as BZY20 – *n* NiO (*n* = 0.5, 1, 2, 5, 10). The mixtures were ball-milled for 10 h, and pressed into pellets at 392 MPa. Pellet-like samples were heated to 1400 or 1600 ^{o}C in ambient atmosphere at a heating rate of 4 ^{o}Cmin^{-1}, and then kept for 24 h for sintering. Samples were finally furnace-cooled to room temperature.

In order to observe the dependence of sintering behavior on the sintering temperature and time, samples of BZY20 – 1 NiO and – 5 NiO were heat-treated at 1400 or 1600 ^{o}C for different time, and finally quenched in ambient atmosphere. BZY20 without NiO, and the Ba-rich sample of $Ba_{1.2}Zr_{0.8}Y_{0.2}O_{3-\delta}$ were also examined for comparison.

2.2 Characterization

Powder X-ray diffraction (XRD) measurements were performed using Cu *K*α radiation with X'Pert-ProMPD (PANalytical, Netherland). Rietveld refinement was carried out by utilizing a commercial software X'Pert HighScore Plus to determine lattice constants. Chemical compositions were measured by inductively coupled plasma atomic emission spectroscopy (ICP-AES) with SPS4000 (Seiko Instruments Inc., Japan). Microstructures were observed by scanning electron microscopy (SEM) with VE-7800 (Keyence Co., Japan). Local compositions were point-analyzed by energy dispersion X-ray spectroscopy (EDS) with X-Max80 (Oxford, UK), equipped with a scanning transmission electron microscopy (STEM, JEM-2010F, JEOL, Japan).

Karl-Fischer titration method was applied to determine water content in the samples. The

pellet-like samples heat-treated at 1400 or 1600 ^{o}C for sintering were broken into pieces about 2 mm in length, and hydrated in wet O_2 or Ar with a water partial pressure of 0.05 atm for 72 h at 600°C. Readers are referred to our previous work [18] for detailed procedures.

Conductivities of pellet-like samples of BZY20 – 1 NiO and BZY20 – 5 NiO with electroless plated palladium electrodes were performed in wet or dry atmosphere of O_2 or H_2. Water partial pressure in these wet atmospheres was kept at 0.05 atm. The impedance spectra were collected by A. C. impedance spectroscopy in the frequency range from 10 Hz to 7 MHz using a frequency response analyzer (Solartron SI 1260, Solartron Analytical, UK) with applied A. C. voltage of 100 mV at temperature from 600 to 100 ^{o}C.

X-ray absorption near-edge structure (XANES) and extended X-ray absorption fine structure (EXAFS) measurements were performed at the SPring-8 synchrotron radiation facility (Hyoko, Japan) by using a Si(111) double-crystal monochromator at beamline BL14B2. Y *K*-edge and Zr *K*-edge measurements were performed by a transmission mode. A fluorescence mode was used for Ni *K*-edge measurements. All measurements were taken at the temperature of 8 K, and analyzed using Artemis software.

3. Results

3.1 Composition analysis

Determined by ICP-AES, as shown in Fig. 1, the actual content of Ni in the samples after being

heat-treated at 1400 and 1600 ^{o}C increased with the increasing nominal content of NiO additive, but certain degree of Ni loss was confirmed,. Fig. 2(a) shows a dark field STEM (DF-STEM) image of BZY20 – 5 NiO heat-treated at 1600 ^{o}C. By STEM-EDS elemental mapping analysis (Fig. 2(b) to (e)), a residue of NiO was confirmed at the triple junction among the BZY20 crystal grains. And obviously different Ni cation ratios of 0.74 at% and 1.30 at%, which were average values by probing more than ten different positions by STEM-EDS point analysis, were determined for intra-grain (dark contrast) and grain boundary (bright contrast), respectively (an example for measured composition is given in Fig. S1 and Table S1). It can be concluded that solubility of Ni in the crystal grain of BZY20 is quite limited, and excessive Ni remains as NiO, or distributes at grain boundary. A similar result was also measured for BZY20 – 5 NiO heat-treated at 1400 ^{o}C with an intra-grain Ni ratio of 0.59 at%.

3.2 Lattice constant

By XRD analysis (as shown in Fig. S2 and S3), only diffraction peaks belonging to a perovskite phase were observed for the sample heat-treated at 1600 ^{o}C, regardless of the NiO content. Although residue of NiO was observed by STEM for BZY20 – 5 NiO, the positions of diffraction peaks of NiO are very close to those of BZY20 [10], and the amount of NiO residue was probably too small to be detected by XRD analysis. When heat-treating at 1400 ^{o}C, a single perovskite phase was confirmed at low NiO content, but diffraction peaks belonging to BaY_2NiO_5 was observed in

BZY20 – 10 NiO.

Lattice constant of the perovskite phase ($Pm\bar{3}m$ [19, 20]) was plotted in Fig. 3. The lattice constant of BZY20 without NiO additive heat-treated at 1400 °C is smaller than that heat-treated at 1600 °C, which is in accordance with our previous report. [21] However, when NiO is added, even with a very small molar ratio of 0.5, the lattice constant increased obviously after heat-treating at 1400 °C. For BZY20 added with the same NiO content, very close lattice constants were obtained for the samples heat-treated at 1400 and 1600 °C. In addition, with the increasing NiO content, the lattice constant decreased.

The sintered samples were ground into powder, and kept in H_2 at 600 °C for 24 h. The lattice constant increased slightly for the BZY20 samples without NiO additive, which is considered to be attributed to a water-incorporated chemical expansion, since the H_2 atmosphere was not absolutely free of water vapor. [20-22] However, after the heat-treatment in H_2, the lattice constant of the samples added with NiO increased greatly, which is obviously beyond the influence by water incorporation.

3.3 Water content

Water content of BZY20 added with different NiO content is shown in Fig. 4. The samples sintered at 1400 °C have larger water content than those sintered at 1600 °C. With the increasing NiO content, the water content decreased, indicating a negative effect of NiO additive on hydration

process. In addition, hydration behavior was different between hydration in wet O_2 and wet Ar. Larger water content was measured when the samples added with NiO were hydrated in wet Ar than wet O_2.

3.4 Microstructure observation by SEM

In order to observe the influence of NiO on sintering behavior by adding NiO, the samples were heat-treated at 1400 and 1600 ^oC for various time, and finally quenched in the ambient atmosphere. The sinterability was poor for pure BZY20 at 1400 ^oC, but got improved with NiO additive. And larger grain was obtained with larger amount of NiO additive (SEM images of the cross-section of the samples kept at 1400 and 1600 ^oC are given in Fig. S4 and S5, respectively). However, regardless of adding NiO, dense morphology and grain growth was confirmed for BZY20 heat-treated at 1600 ^oC. These results were in well agreement with previous studies. [14, 15]

Very interesting morphologies were observed for the Ba-rich sample of $Ba_{1.2}Zr_{0.8}Y_{0.2}O_{3-\delta}$ without NiO addition. For the sample heat-treated at 1600 ^oC for 24 h, as shown in Fig. 5(a), it is quite clear that a step-like morphology formed with a spherical top end. In the light of reported pseudoternary phase diagrams of BaO - ZrO_2 - $YO_{1.5}$ at 1600 ^oC, this Ba-rich composition of $Ba_{1.2}Zr_{0.8}Y_{0.2}O_{3-\delta}$ resides in the region equilibrating with a liquid phase [23, 24]. This step-like morphology should be attributed to the gradually cooling and solidification of the liquid phase. A similar morphology was also observed for the sample heat-treated at 1400 ^oC, as shown in Fig. 5(b).

Some interesting morphologies were also confirmed in the sample of NiO-added BZY20 heat-treated at 1600 ^{o}C. Fine spherical particles were observed along the grain boundary of BZY20 -1 NiO (Fig. 5(c)). And a microstructure with round edge, which is obviously different from ordinary BZY20 grains, was confirmed in BZY20 – 5 NiO (Fig. 5(d)).

3.5 Conductivity

The bulk (intra-grain) conductivity of BZY20 – 1 NiO and - 5 NiO, which were sintered at 1400 and 1600 ^{o}C, are shown in Fig. 6. When the smaller NiO content was added, the bulk conductivities in wet H_2 and wet O_2 are very close to that of the pure BZY20 in wet H_2. When the atmosphere was altered to a dry one, the conductivity decreased obviously, indicating that proton conduction still dominated. However, in the sample of BZY20 – 5 NiO, the conduction behavior changed greatly. Although the conductivity is still higher in a wet atmosphere than in a dry one, it dropped about a magnitude of two orders comparing with that of the pure BZY20.

As shown in Fig. 7, the samples heat-treated at 1600 ^{o}C have a higher grain boundary conducitivity than those heat-treated at 1400 ^{o}C, due to the larger grain size obtained at a higher sintering temperature. For the samples heat-treated at the same temperature of 1400 ^{o}C, BZY20 – 5 NiO had a little bit higher grain boundary conductivity than that of BZY20 – 1 NiO, due to the improved sinterability with increased NiO additive (Fig. S4(c) and (d)). However, when the samples were heat-treated at 1600 ^{o}C, the grain boundary conductivity of BZY20 – 1 NiO became

higher than that of BZY20 – 5 NiO. The concentration of the excessive Ni at the grain boundary might turn to be the predominant factor, since the greatly enlarged gain sizes of both BZY20 – 1 NiO and 5 NiO (S5(c) and (d)) made the difference in grain size effect small.

3.6 Relationship between lattice constants and sintering behavior

Time variation of XRD patterns gives meaningful information. (011) diffraction peak is focused for example and listed in Fig. 8 and 9, showing the cases for heat-treating at 1600 and 1400 ^{o}C, respectively. For the pure BZY20 as-synthesized at 1300 ^{o}C, as shown in Fig. 8(a), the vertex of (011) peak located at about 30.15 degree. When the temperature was just heated up to 1600 ^{o}C at the rate of 4 ^{o}Cmin^{-1}, and held for 0 h, another diffraction peak appeared at a relatively low angle side, and coexisted with the weakened peak around 30.15 degree. After the sample was heat-treated for more than 2 h, only the peak at the low angle side remained. The change of the peak shape of $Ba_{1.2}Zr_{0.8}Y_{0.2}O_{3-\delta}$ (Fig. 8(b)) behaves similarly. Referring to the samples added with NiO, as shown in Fig. 8(c) and 8(d), even at the time when the temperature just achieved 1600 ^{o}C (namely, keeping at 1600 ^{o}C for 0 h), only the peak at the relatively low angles side remained. And the peak split due to radiations of Cu *K*α1 and Cu *K*α2. These results clearly indicate that there are two phases for Y-doped $BaZrO_3$. One has a small lattice constant, whereas another has a large one. By elevating the temperature, such as from 1300 to 1600 ^{o}C, the phase with a large lattice constant appeared. And adding NiO seems to promote the formation of such phase.

Different phenomenon was observed when the sintering temperature was lowered from 1600 to 1400 °C. As shown in Fig. 9(a), even the BZY20 sample was kept at 1400 °C for 24 h, there was no obvious change in the (011) peak shape. For the $Ba_{1.2}Zr_{0.8}Y_{0.2}O_{3-\delta}$ sample, as shown in Fig. 9(b), the peak shape changed little after heating at 1400 °C for 2 h, but a diffraction peak at the relatively small angle side appeared after heating for 4 h. And the intensity of this new peak increased with the time. The formation rate was much slower than that at 1600 °C. The phase formation with a large lattice constant was also confirmed for the samples added with NiO. A certain correlation existed between the sintering and phase behaviors. Although the clarification of such correlation is beyond the scope of the present work, it is reasonable to suggest that the sintering and change of the phase might proceed in a related way (the lattice constants of the perovskite phases in these samples were plotted in Fig. S6 and S7).

3.7 EXAFS analysis

Detailed information on local structure is obtained by EXAFS measurements. For the sake of simplicity, we here only used the sample of BZY20 – 1 NiO, in which the actual cation ratios of Ni were 0.40 and 0.39 at% after being heat-treated at 1400 and 1600 °C, respectively, less than the expected intra-grain solubility of Ni. Fitting of EXAFS data collected at Zr *K*-edge and Y *K*-edge is given in the Supplementary Information. For fitting the BZY20 – 1 NiO heated at 1400 °C at Ni *K*-edge, best fit was achieved by using a model with Ni locating at the position of $(\frac{1}{2}, 0, 0)$, as given

in the inset of Fig. 10. In this fitting, a three-shell structure was adopted as follows: (1) Ni – O first shell; (2) Ni – Ba second shell; (3) Ni- Zr/Y third shell. The fittings of the EXAFS data in *k*-space and the Fourier-transformed data in *R*-space are shown in Fig. 10 and 11, respectively. The results are listed in Table 1. For the Ni – Ba shell, its coordination number is determined to be 0.29, greatly smaller than the theoretical value of 2. This is reasonable because of a strong repulsion force between positively charged Ba and Ni cations. As the result of such Ni occupancy, structural distortion was induced. The distances of Ni – O, Ni – Ba and Ni – Zr/Y were determined to be 1.88, 2.35 and 3.10 Å, respectively, significantly different from 2.11, 2.11 and 2.98 Å of BZY20 without NiO addition. A comparison of the Fourier-transformed Ni *K*-edge EXAFS data of BZY20 – 1 NiO as-sintered at 1400 or 1600 ^{o}C, and subsequently heated at 600 ^{o}C in H_2 was shown in Fig. 12. After the samples were heat-treated in H_2, the profile obviously changed.

However, fitting the data of the samples after heat-treatment in H_2, and also the one sintered at 1600 ^{o}C, did not lead to sufficiently reasonable results by using the structure model of Ni at ($\frac{1}{2}$, 0, 0) position. We also attempted the structure models of occupation of Ni at the Zr-site of ($\frac{1}{2}$,$\frac{1}{2}$,$\frac{1}{2}$), Ba-site of (0, 0, 0), and some known Ni substances (Ni metal, NiO, BaY_2NiO_5), as well as the combinations of these models, but cannot improve the fitting quality. Some other possibility, in addition to those mentioned in this work, may coexist, and expects a further investigation.

3.8 XANES spectra

XANES spectra for the BZY20 – 1 NiO samples heat-treated at 1400 and 1600 ^{o}C in air, and subsequently heat-treated at 600 ^{o}C in H_2 are shown in Fig. 13. It is clear that the rising-edge of the absorption profile shifted towards the low energy side for the samples heat-treated in H_2, indicating the decrease of oxidation state of Ni. Quantitatively estimating the oxidation state of Ni is possible based on several excellent works. [25, 26] O'Grady *et al*. reported that a good correlation can be established between the Ni *K*-edge absorption energy and the oxidation state of Ni. [26] And recently, Woolley *et al*. applied such correlation, and successfully determined the oxidation state of Ni in a composite oxide containing La and Ni. [26] We here adopted the same methodology. The Ni *K*-edge positions of BZY20 – 1 NiO, and standard samples of Ni and NiO, were manually determined as the maximum in the first derivative data, and were listed in Table 2. Then the Ni *K*-edge positions of Ni and NiO in our measurements, and $BaNiO_3$ containing tetravalent Ni reported by O'Grady *et al*. [25], were plotted against the oxidation state of Ni in Fig. 14. With the calibration curve, the oxidation state of BZY20 – 1 NiO after heat-treated in air at 1400 and 1600 ^{o}C were estimated to be 2.89 and 2.80, respectively, which reduced to 2.80 and 2.60 after being kept in H_2 at 600 ^{o}C. These quantitative analyses imply that Ni introduced into BZY20 is mainly trivalent, and can be partially reduced towards divalent in H_2 at 600 ^{o}C. Reduction to a lower oxidation state usually results in an increase of the radius of Ni cations [27], which gives an answer to the increased lattice constant of the samples added with NiO after being kept in H_2 at 600 ^{o}C, as shown in Fig. 3.

4. Discussion

Ni was determined to be mainly trivalent, and occupy the interstitial position of ($\frac{1}{2}$, 0, 0) in BZY20 - 1 NiO which was heat-treated in air at 1400 °C. Taking the Ba loss around Ni from 2 to 0.29 into consideration, the reaction between BZY20 and NiO, with a molar ratio of 100 : 1, can be written using a Krönig-Vink notation as Eq. (1), which indicates that by interstitially introducing trivalent Ni cations ($Ni_i^{\bullet\bullet\bullet}$) into the lattice of BZY20, oxide ion vacancies ($V_O^{\bullet\bullet}$) and Ba-site vacancies ($V_{Ba}^{''}$) generate.

$$4NiO + 6.84Ba_{Ba}^{\times} + 0.84O_O^{\times} + O_2 \rightarrow 4Ni_i^{\bullet\bullet\bullet} + 6.84V_{Ba}^{''} + 0.84V_O^{\bullet\bullet} + 6.84BaO \quad (1)$$

$$H_2O + V_O^{\bullet\bullet} + O_O^{\times} \rightarrow 2OH_O^{\bullet} \quad (2)$$

Although increasing the oxide ion vacancies favors the proton introduction as indicated in Eq. (2), the formation of Ba-site vacancies is known to be detrimental to the proton conduction [28]. Therefore, it can be expected that with the increasing content of NiO additive, the concentration of Ba-site vacancies increases, and the proton conductivity consequently decreases, which is in very well agreement with the experimental observation in this work. And it is reasonable to believe that the predominated intra-grain location of Ni, even at 1600 °C, should be the interstitial position of ($\frac{1}{2}$, 0, 0).

Improving the sinterability of BZY20 is a very attractive property of NiO. A sintering mechanism was suggested by Tong *et al*. that by addition of NiO, BaY_2NiO_5 formed during heating and subsequently decomposed to form a liquid phase, which benefits the sintering. [16, 17] Based on

our experimental observation comparing the sintering behavior of $Ba_{1.2}Zr_{0.8}Y_{0.2}O_{3-\delta}$ with BZY20, we agree that the formation of liquid phase is a key for improving the sinterability. However, we did not observe the formation of BaY_2NiO_5 from the XRD patterns of BZY20 – *n* NiO (*n* = 1, 5) heat-treated at 1400 and 1600 ^{o}C from 0 to 24 h.

Instead, a new hypothesis can be suggested. When the temperature was lowered to 1400 ^{o}C, BZY20 without NiO cannot be sintered. But after keeping at 1400 ^{o}C for 4 h, in the sample of $Ba_{1.2}Zr_{0.8}Y_{0.2}O_{3-\delta}$, grain growth can also be confirmed (Fig. S4(b)). $Ba_{1.2}Zr_{0.8}Y_{0.2}O_{3-\delta}$ is Ba-rich, and a liquid phase forms even at 1400 ^{o}C (Fig. 5(b)), which should be the reason for its better sinterability. The liquid phase was also confirmed in the mixture of BZY20 and NiO after being heat-treated at 1600 ^{o}C (Fig. 5(c) and (d)). Unfortunately, we did not directly observe the liquid phase for the NiO-added samples at 1400 ^{o}C, because the grain size was not large sufficiently and made the SEM observation of grain boundary very difficult. By EXAFS measurements, Ba-deficiency was determined around the Ni cations, indicating that Ba cations were driven to the grain boundary, which then became relatively Ba-rich. A Ba-rich grain boundary should facilitate the formation of a liquid phase. We here suggest that occupying the interstitial position, such as $(\frac{1}{2}, 0, 0)$, by Ni cations, is the origin of the formation of the liquid phase, and thereby the improvement of sinterability.

5. Conclusions

In this work, a systematic investigation was performed on the BZY20 samples added with and without NiO. The results revealed that with the increasing content of NiO additive, the water content and the conductivity of the samples which were sintered at 1400 and 1600 °C decreased. It is because Ni cations, which were mainly trivalent, occupied the interstitial position of ($\frac{1}{2}$, 0, 0) in the lattice of BZY20. Such location of Ni cations might be detrimental to water incorporation and proton conduction. The behavior of NiO as a sintering aid for BZY20 is also greatly related to such occupancy of NiO. By incorporation of Ni cations into the ($\frac{1}{2}$, 0, 0) position, a loss of Ba cations surrounding the Ni cations occurs. It is suggested that these Ba cations were driven to the grain boundary, and induced the formation of a liquid phase, which promoted the sintering process. In summary, occupying the ($\frac{1}{2}$, 0, 0) interstitial position by Ni cations improved the sinterability of BZY20, but also negatively influenced the proton conduction.

Acknowledgements

This study was supported by Innovation Promotion Project (P07026) from the New Energy and Industrial Technology Development Organization (NEDO) of Japan. XANES and EXAFS measurements were performed at the SPring-8 synchrotron radiation facility (Hyogo, Japan) with the approval of the Japan Synchrotron Radiation Research Institute (JASRI) as industrial application proposal (No. 2013B1568).

References

1 W. Grover Coors, *J. Power Sources*, 2003, **118**, 150.

2 Y. Yamazaki, R. Hernandez-Sanchez and S.M. Haile, *Chem. Mater*., 2009, **21**, 2755.

3 D. Pergolesi, E. Fabbri, A. D'Epifanio, E.D. Bartolomeo, A. Tebano, S. Sanna, S. Licoccia, G. Balestrino and E. Traversa, *Nat. Mater*., 2010, **9**, 846.

4 D. Han, Y. Nose, K. Shinoda, T. Uda, *Solid State Ionics*, 2012, **213**, 2.

5 Y. Okumura, Y. Nose, J. Katayama, T. Uda, *J. Electrochem. Soc*., 2011, **158**, B1067.

6 J. Shim, J. Park, J. An, T.M. Gür, S. Kang, F.B. Printz, *Chem. Mater*., 2009, **21**, 3290.

7 Y. Guo, Y. Lin, R. Ran, Z. Shao, *J. Power Sources*, 2009, **193**, 400.

8 W. Sun, L. Yan, Z. Shi, Z. Zhu, W. Liu, *J. Power Sources*, 2010, **195**, 4277.

9 L. Bi, E. Fabbri, Z. Sun, E. Traversa, *Energy Environ. Sci*., 2011, **4**, 409.

10 L. Bi, E. Fabbri, Z. Sun, E. Traversa, *Energy Environ. Sci*., 2011, **4**, 1352.

11 D. Pergolesi, E. Fabbri, E. Traversa, *Electrochem. Commun*., 2010, **12**, 977.

12 S. Robinson, A. Manerbino, W. Grover Coors, N.P. Sullivan, *Fuel Cells*, 2013, **4**, 584.

13 P. Babilo, S.M. Haile, *J. Am. Ceram. Soc*., 2005, **88**, 2362.

14 S. Imashuku, T. Uda, Y. Nose, K. Kishida, S. Harada, H. Inui, Y. Awakura, *J. Electrochem. Soc*., 2008, **155**, B581.

15 J. Tong, D. Clark, M. Hoban, R. O'Hayre, *Solid State Ionics*, 2010, **181**, 496.

16 J. Tong, D. Clark, L. Bernau, M. Sanders, R. O'Hayre, *J. Mater. Chem*., 2010, **20**, 6333.

17 S. Nikodemski, J. Tong, R. O'Hayre, *Solid State Ionics*, 2013, **253**, 201.

18 D. Han, Y. Okumura, Y. Nose, T. Uda, *Solid State Ionics*, 2010, **181**, 1601.

19 D. Han, K. Kishida, K. Shinoda, H. Inui, T. Uda, *J. Mater. Chem. A*, 2013, **1**, 3027.

20 D. Han, K. Shinoda, T. Uda, *J. Am. Ceram. Soc*., 2014, **97**, 643.

21 C. Hiraiwa, D. Han, A. Kuramitsu, A. Kuwabara, H. Takeuchi, M. Majima and T. Uda, *J. Am. Ceram. Soc*., 2013, **96**, 879.

22. D. Han, M. Majima and T. Uda, *J. Solid State Chem*., 2013, **205**, 122.

23 S. Imashuku, T. Uda, Y. Nose and Y. Awakura, *J. Phase Equilib. Diff*., 2010, **31**, 348.

24 Y. Oyama, A. Kojima, R.B. Cervera, K. Tanaka, S. Yamaguchi, *Solid State Ionics*, 2011, **197**, 1.

25 W.E. O'Grady, K.I. Pandya, K.E. Swider, D.A. Corrigan, *J. Electrochem. Soc*., 1996, **143**, 1613.

26. R.J. Woolley, B.N. Illy, M.P. Ryan, S.J. Skinner, *J. Mater. Chem*., 2011, **21**, 18592.

27 R.D. Shannon, *Acta Crystallogr. Sect. A*, 1976, **32**, 751.

28 Y. Yamazaki, R. Hernandez-Sanchez and S.M. Haile, *J. Mater. Chem*., 2010, **20**, 8158.

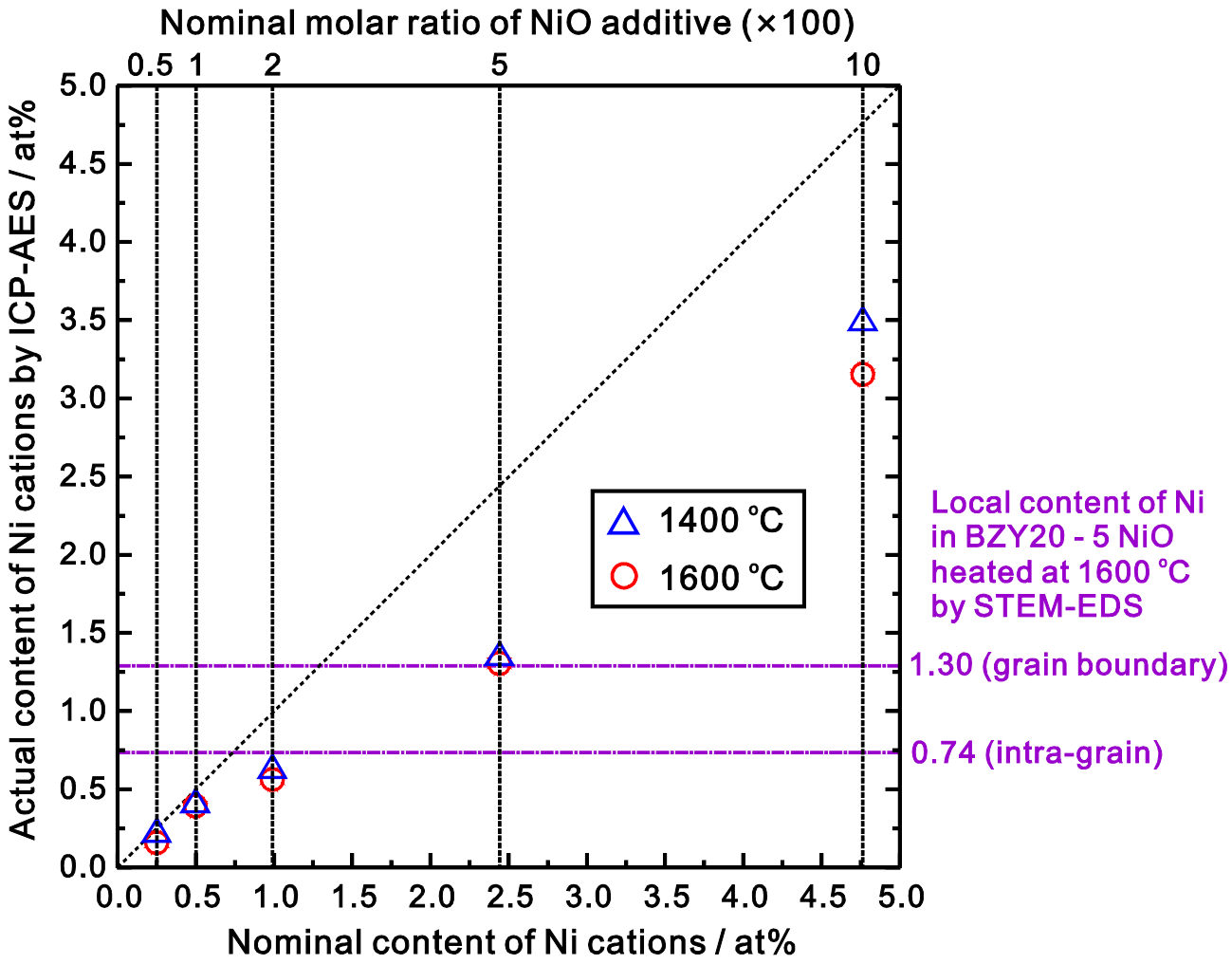

Fig. 1 Cation ratio of Ni determined by ICP-AES plotted against the nominal content of Ni cations. Loss of Ni was observed after the heat-treatment in 1400 and 1600 ºC in air for 24 h. The top abscissa indicates the nominal molar ratio of NiO additive against BZY20.

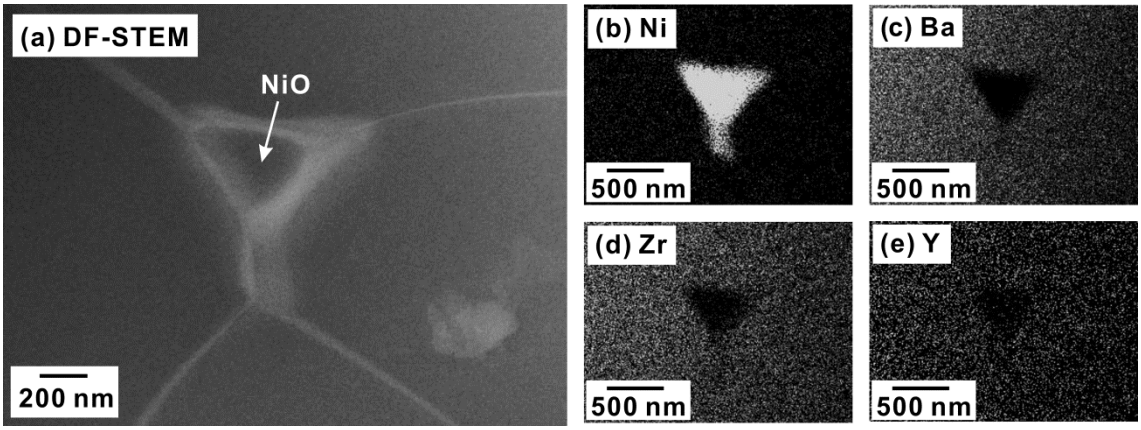

Fig. 2 (a) A DF-STEM image of BZY20 - 5 NiO, which was heat-treated at 1600 ºC in air for 24 h, and distribution of (b) Ni, (c) Ba, (d) Zr, and (e) Y by STEM-EDS elemental mapping analysis..

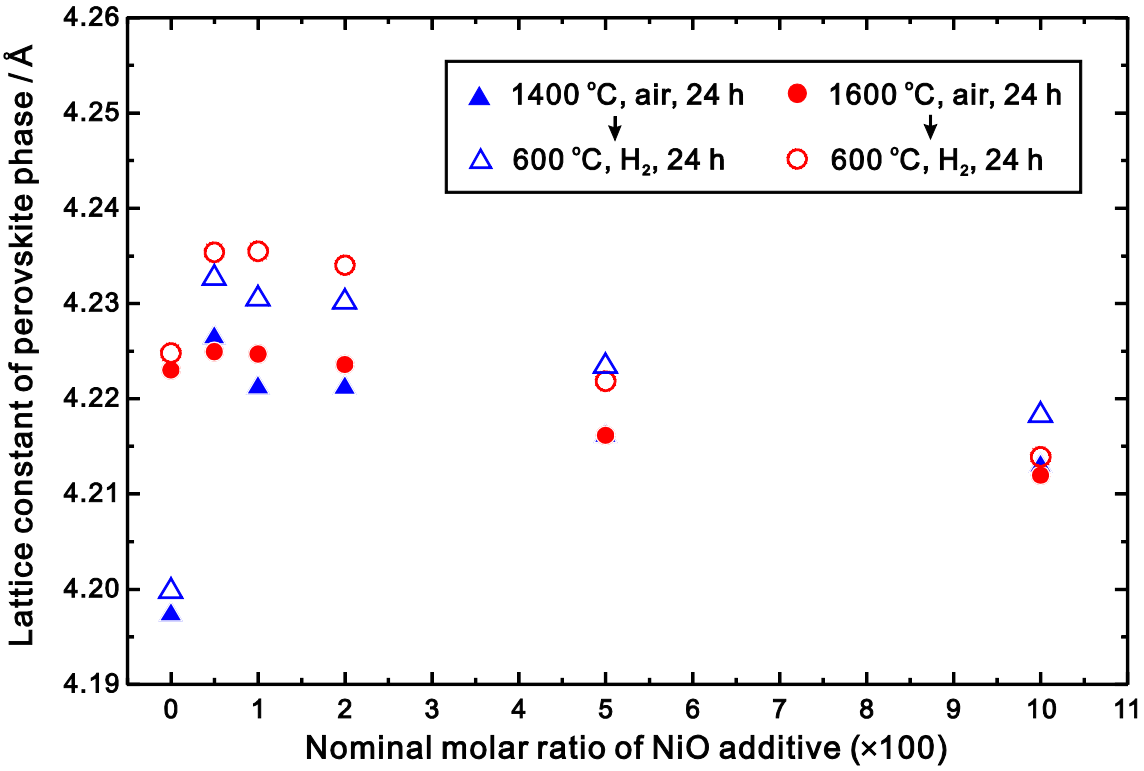

Fig. 3 Lattice constant of the perovskite phases ($Pm\bar{3}m$) in BZY20 mixing with various content of NiO. Samples were heat-treated at 1400 °C or 1600 °C in air for 24 h for sintering, and then kept in H_2 at 600 °C for 24 h. The abscissa indicates the nominal molar ratio of NiO additive against BZY20.

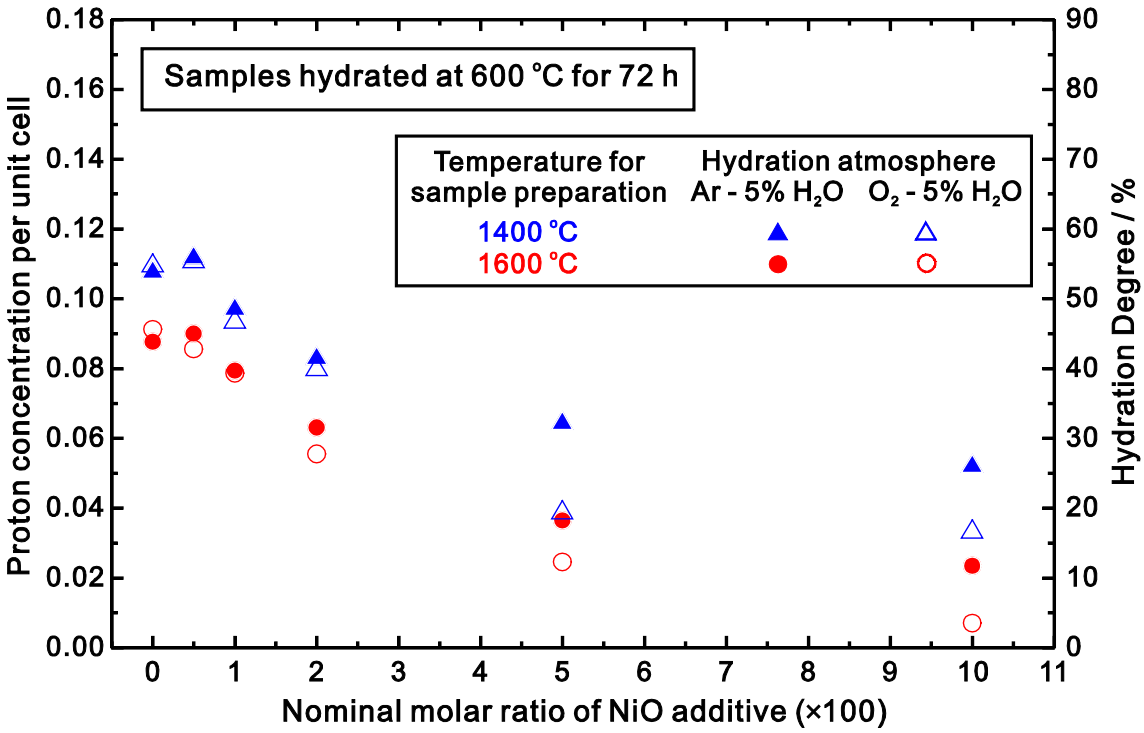

Fig. 4 Water content of BZY20 mixing with various content of NiO, determined by Karl-Fischer titration method. Samples were heat-treated at 1400 °C or 1600 °C in air for 24 for sintering, then hydrated in wet O_2 or wet Ar with water partial pressure of 0.05 atm for 72 h. The abscissa indicates the nominal molar ratio of NiO additive against BZY20.

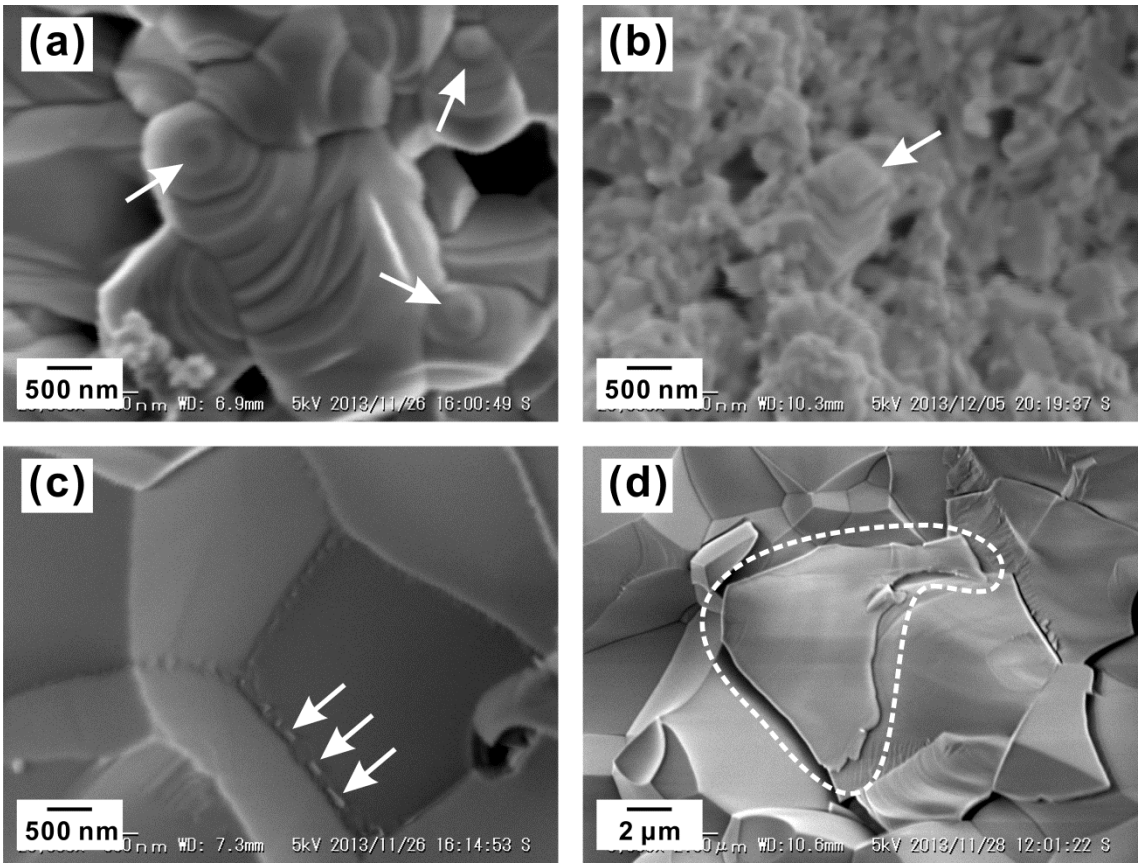

Fig. 5 SEM images of trace of liquid phase marked by arrows in $Ba_{1.2}Z_{0.8}Y_{0.2}O_{3-\delta}$ heat-treated at (a) 1600 ºC, and (b) 1400 ºC in air for 24 h, and (c) BZY20 – 1 NiO heat-treated at 1600 ºC for 24 h, and highlighted by a dashed circle in (d) BZY20 – 5 NiO heat-treated at 1600 ºC for 16 h. All the samples were finally quenched in ambient atmosphere.

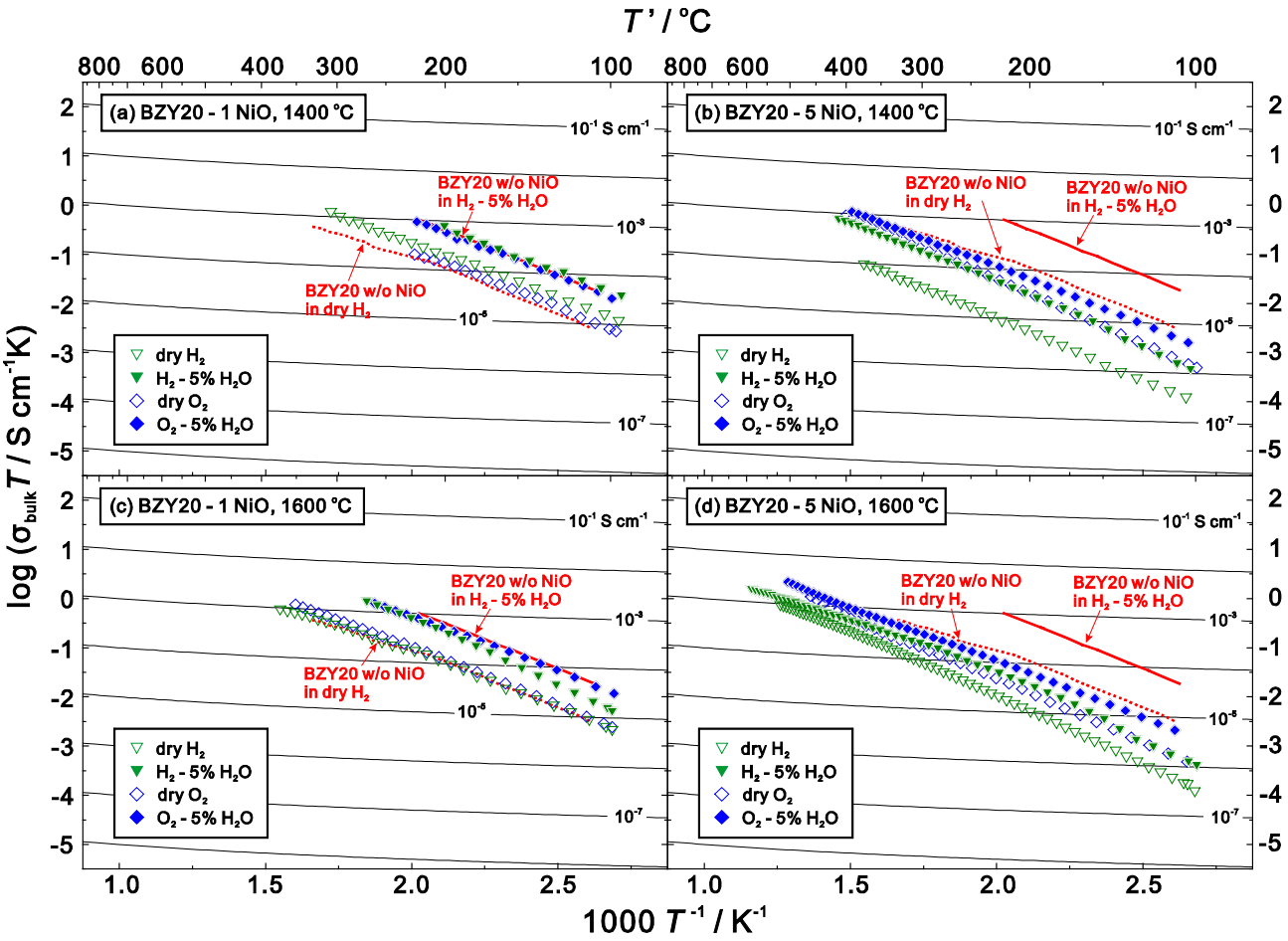

Fig. 6 Bulk (intra-grain) conductivities of BZY20 - 1 NiO and 5 NiO heat-treated at 1400 °C and 1600 °C in air for 24 h. The conductivity were measured in dry H_2 (open triangles), H_2 - 5% H_2O (solid triangles), dry O_2 (open square) and O_2 – 5% H_2O (solid square). Bulk conductivity of BZY20 in dry H_2 (red dash line) and H_2 – 5% H_2O (red solid line) were also plotted for comparison.

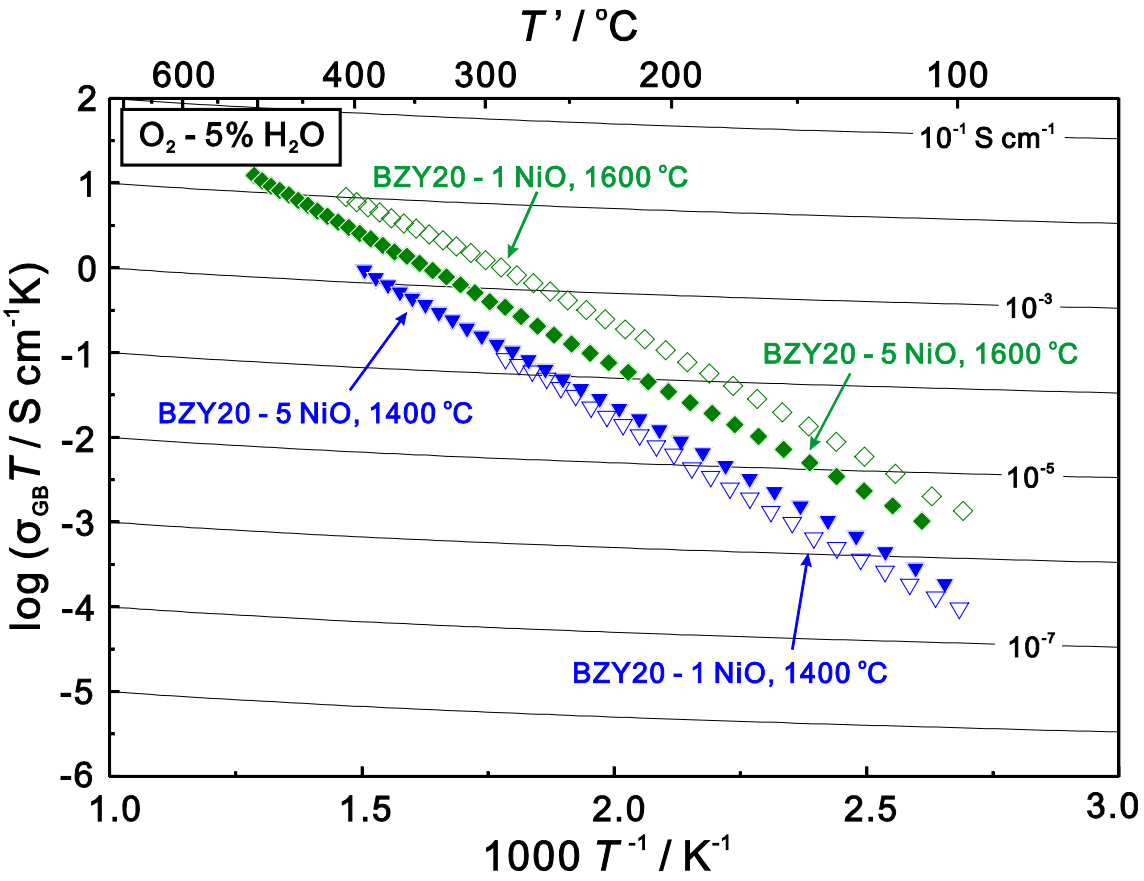

Fig. 7 Grain boundary conductivity of BZY20 - 1 NiO and 5 NiO in O_2 – 5% H_2O. Samples were heat-treated at 1400 or 1600 °C in air for 24 h.

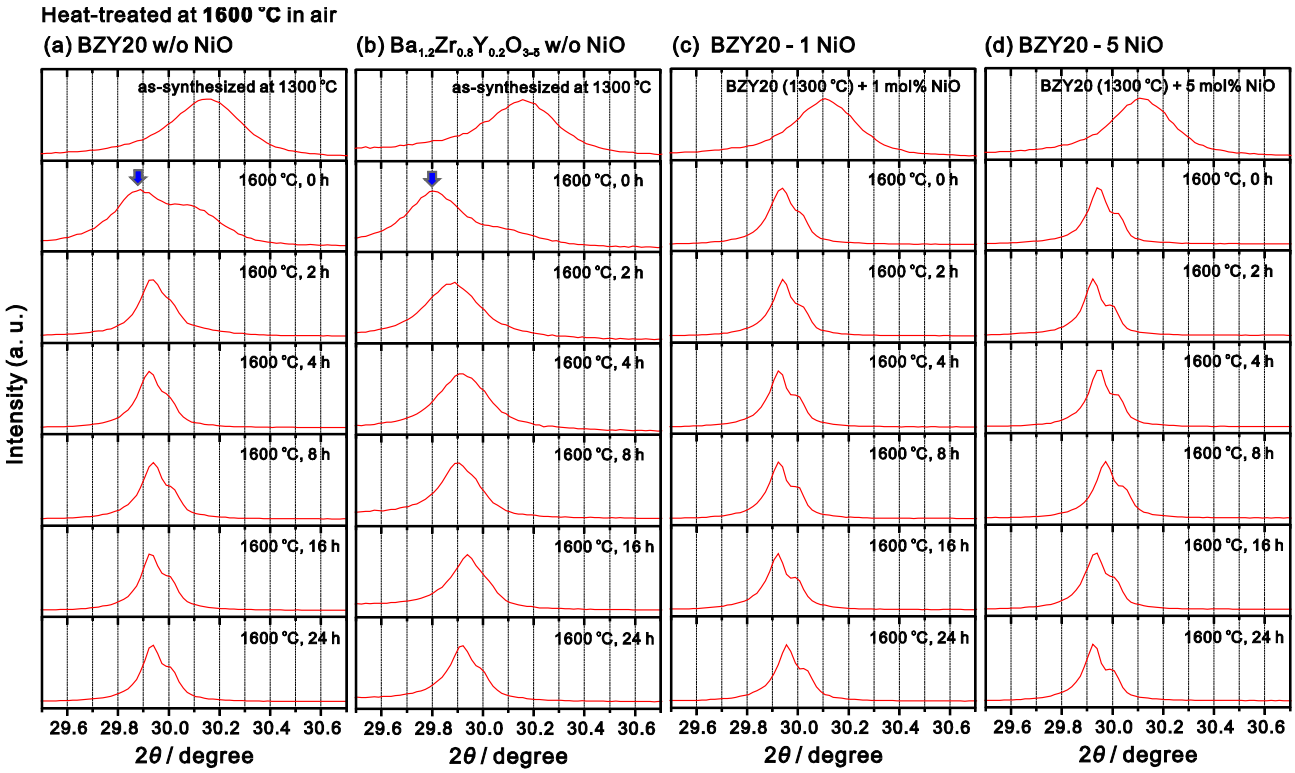

Fig. 8 Variation of (011) diffraction peak shape of (a) BZY20, (b) $Ba_{1.2}Zr_{0.8}Y_{0.2}O_{3-\delta}$, (c) BZY20 – 1 NiO, and (d) BZY20 – 5 NiO, which were heat-treated at 1600 ^{o}C in air for different time. The samples were finally quenched in ambient atmosphere.

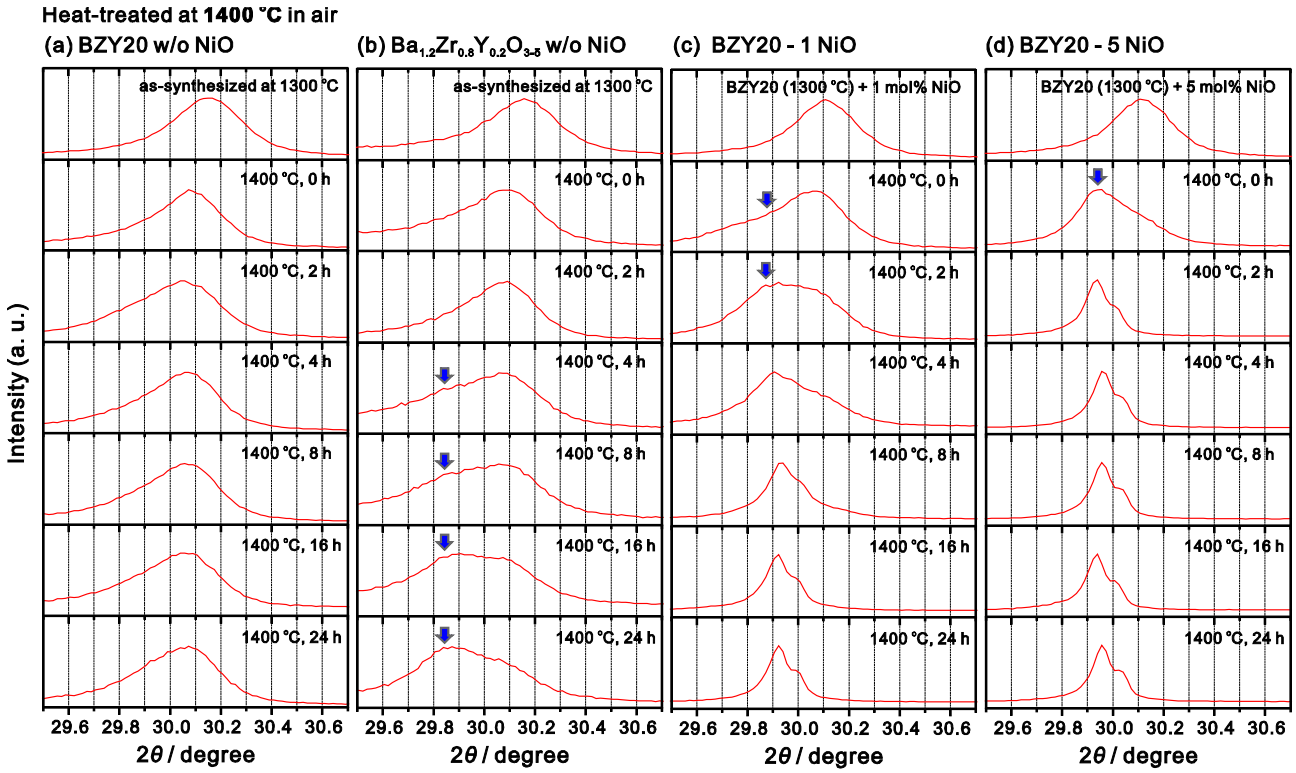

Fig. 9 Variation of (011) diffraction peak shape of (a) BZY20, (b) $Ba_{1.2}Zr_{0.8}Y_{0.2}O_{3-\delta}$, (c) BZY20 – 1 NiO, and (d) BZY20 – 5 NiO, which were heat-treated at 1400 ^{o}C in air for different time. The samples were finally quenched in ambient atmosphere.

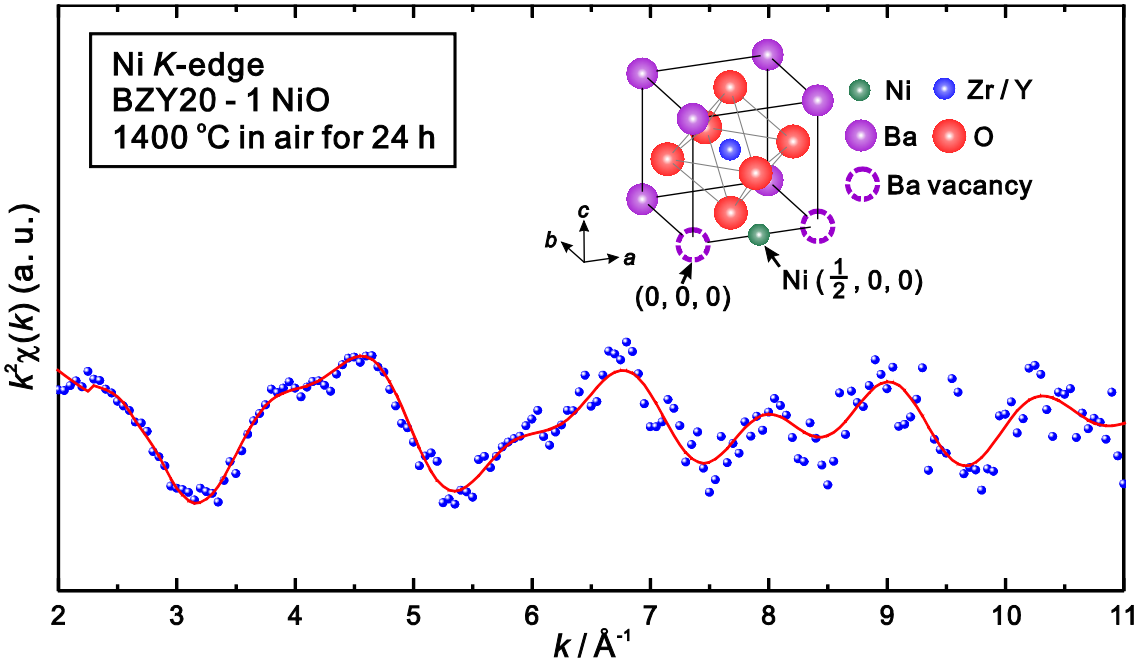

Fig. 10 Ni *K*-edge EXAFS data (circles) and best fit (red line) of BZY20 – 1 NiO heat-treated at 1400 °C in air for 24 h. Inset gives the model used in the fitting which has Ni cations occupying (0.5, 0, 0) position. Data were collected at 8 K in vacuum.

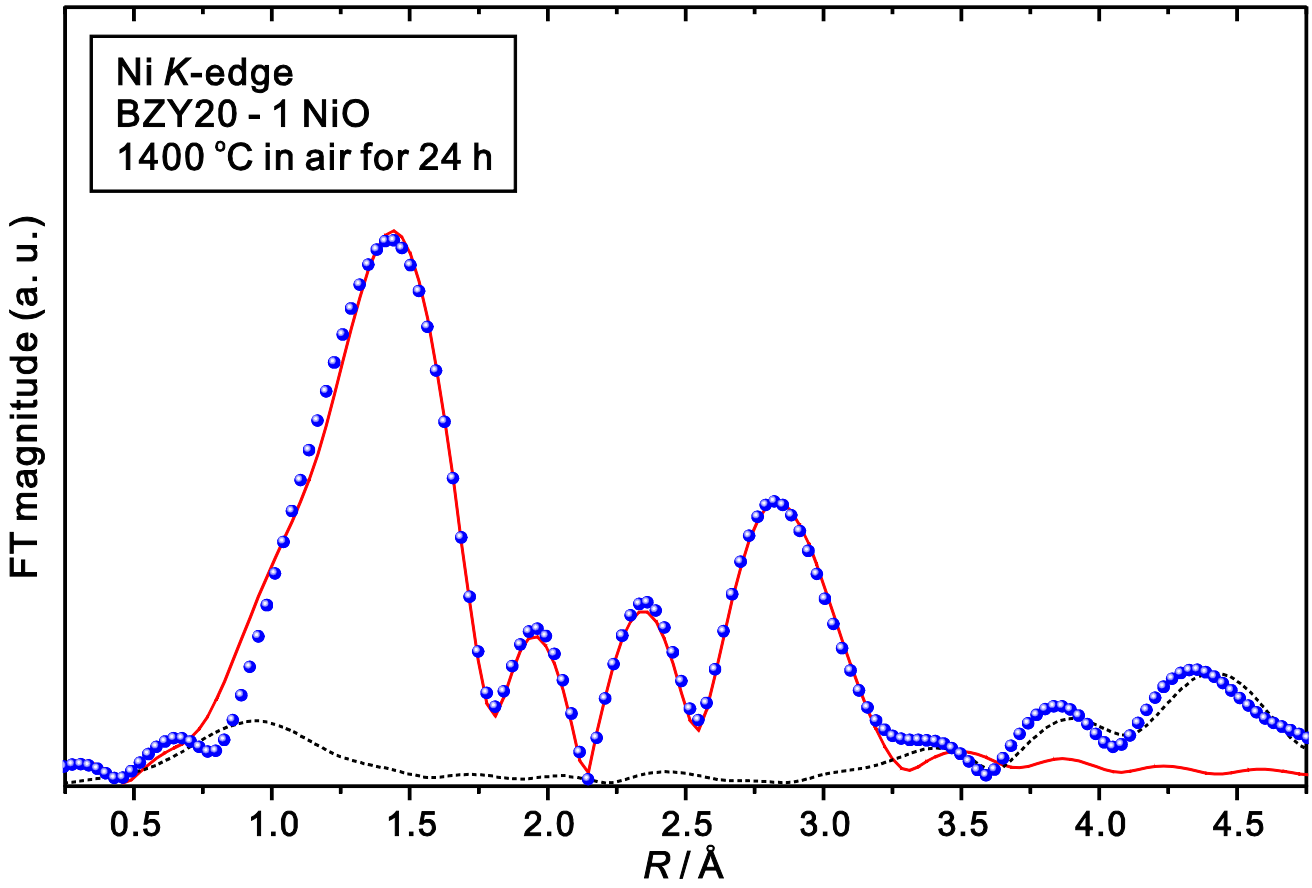

Fig. 11 Fourier-transformed Ni *K*-edge EXAFS data (circles), best fit (solid line), and residual (dash line) of BZY20 – 1 NiO heat-treated at 1400 °C in air for 24 h. Data were collected at 8 K in vacuum.

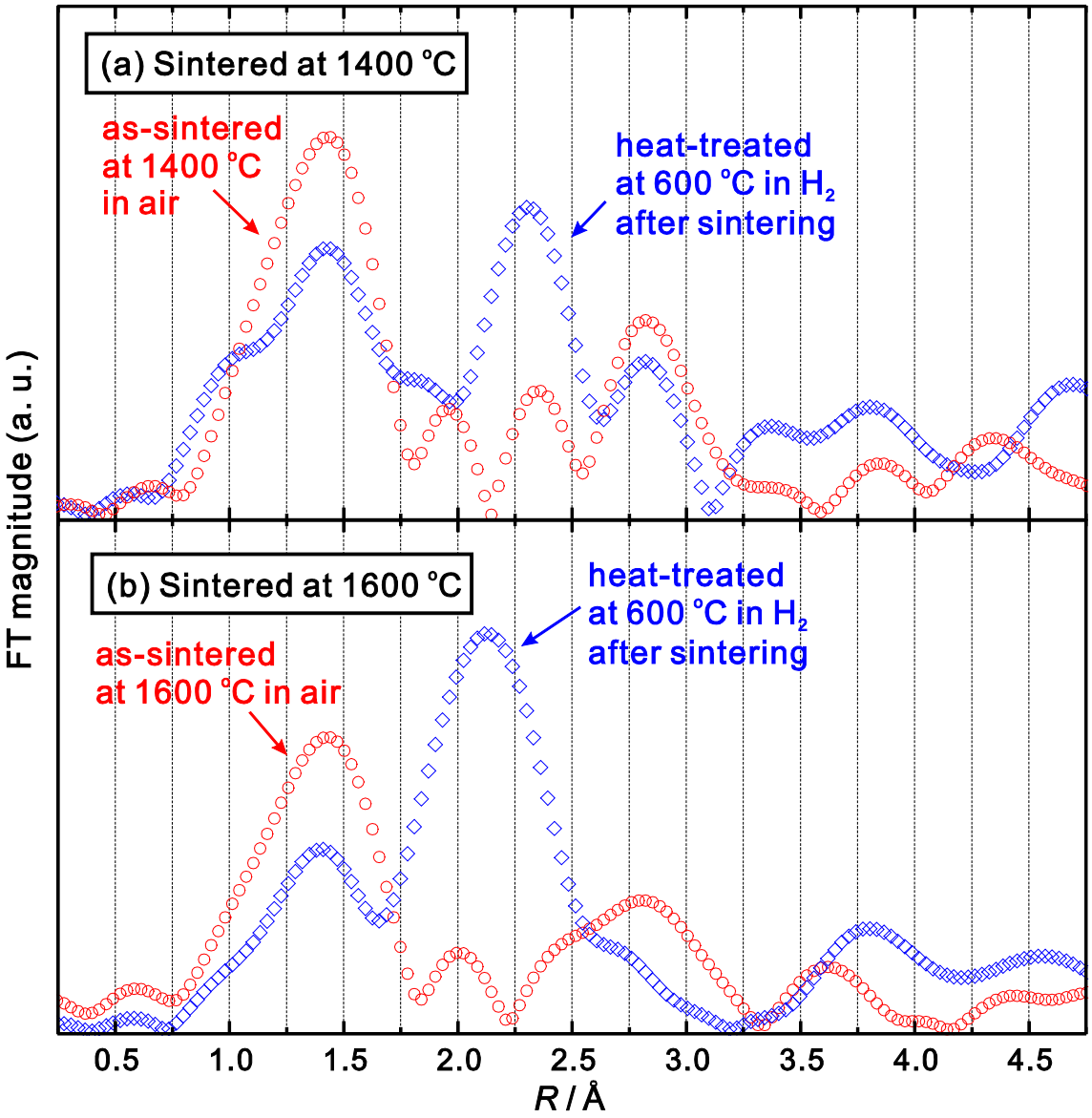

Fig. 12 Comparison of Fourier-transformed Ni *K*-edge EXAFS data of BZY20 – 1 NiO as-sintered at (a) 1400 °C or (b) 1600 °C in air for 24 h, with those subsequently heat-treated at 600 °C in H_2 for 48 h. Data were collected at 8 K in vacuum.

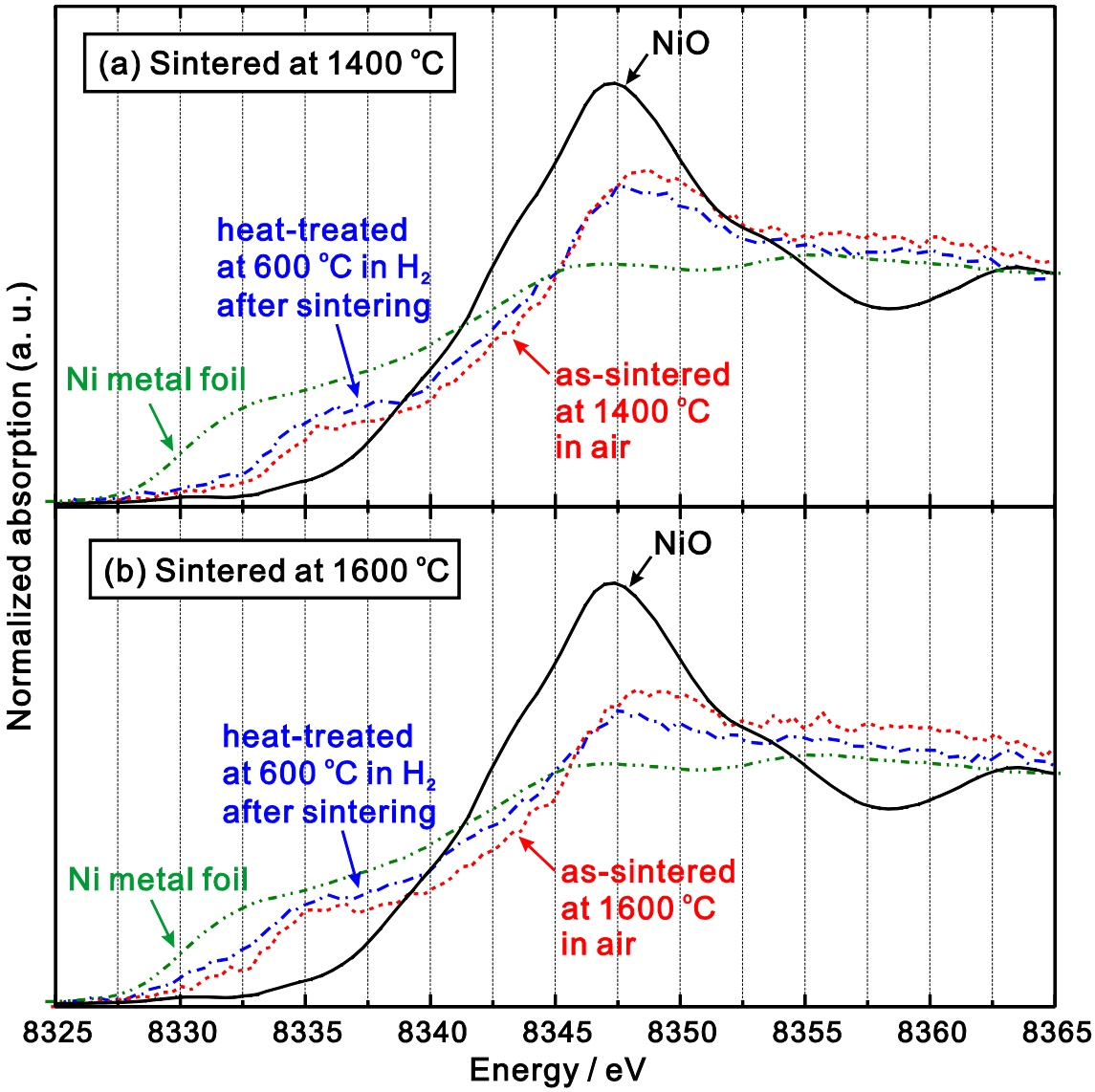

Fig. 13 Ni *K*-edge XANES data obtained for (a) BZY20 – 1 NiO heat-treated at 1400 °C in air for 24 h, and subsequently heat-treated at 600 °C in H_2 for 24 h, and (b) BZY20 – 1 NiO heat-treated at 1600 °C in air for 24 h, and subsequently heat-treated at 600 °C in H_2 for 24 h. XANES data of Ni and NiO are also plotted. Data were collected at 8 K in vacuum.

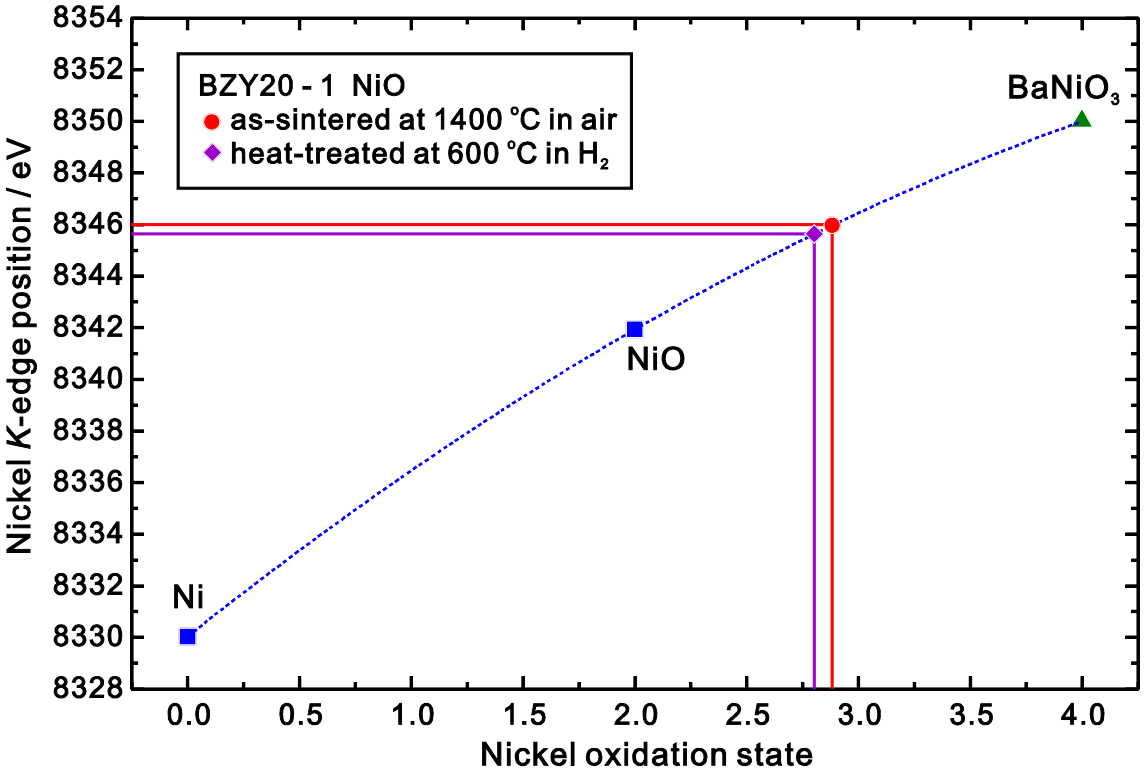

Fig. 14 Nickel oxidation state plotted against Ni *K*-edge position. Ni *K*-edge position of tetravalent Ni ($BaNiO_3$) was reported by O'Grady et al.[26]. A polynomial of degree two (dash curve) was applied for calibration curve. Examples for determining the oxidation state of Ni in $BaZrO_3$ was plotted for example by using the samples of BZY20 – 1 NiO heat-treated at 1400 ^oC in air for 24 h, and 600 ^oC in H_2 for 24 h in sequence.

Table 1 EXAFS results for BZY20 – 1 NiO on the Ni *K*-edge. The sample was heat-treated at 1400 °C in air for 24 h. The EXAFS measurement was performed at 8 K in vacuum.

	R / Å	σ^2 / Å^2	Coordination number	
			Measured value	Theoretical value
Ni – O	1.88	0.0031	3.85(42)	4
Ni – Ba	2.35	0.0076	0.29(3)	2
Ni – Zr/Y	3.10	0.0093	3.92(44)	4

Table 2 Nickel oxidation state and *K*-edge position data.

	Composition	Heat-treatment	Ni *K*-edge position / eV	Ni oxidation state
Standard samples	Ni	-	8330.0	0
	NiO	-	8341.9	2
	$BaNiO_3$ [26]	-	8350.0	4
Samples for measurement	BZY20 – 1 NiO	1400 °C in air for 24 h	8346.0	2.89
		1400 °C in air for 24 h then 600 °C in H_2 for 48 h	8345.6	2.80
		1600 °C in air for 24 h	8345.6	2.80
		1600 °C in air for 24 h then 600 °C in H_2 for 48 h	8344.7	2.60